ELSEVIER

Journal of Physics and Chemistry of Solids 63 (2002) 171–177

JOURNAL OF PHYSICS AND CHEMISTRY OF SOLIDS

www.elsevier.com/locate/jpcs

Influence of initial pH on the particle size and fluorescence properties of the nano scale Eu(III) doped yttria

P.K. Sharma[a,*], M.H. Jilavi[b], V.K. Varadan[a], H. Schmidt[b]

[a]*Center for Engineering of Electronics Acoustic Materials & Devices, Department of Engineering Science & Mechanics, The Pennsylvania State University, 212 Earth & Engineering Science Building, University Park, PA 16802, USA*

[b]*Institut fuer Neue Materialien, Im Stadtwald, Geb.-43, D-66123, Saarbrucken, Germany*

Received 3 October 2000; accepted 2 April 2001

Abstract

Europium doped ytrrium oxide (Eu:Y_2O_3) was synthesized by a chemical wet method in the presence of tween-80 and ϵ-caprolactam in pH range 4–10. It has been observed that the variation in surface area, pore size, and pore volume of the final product, was strongly dependent on the initial pH of the solution. The powder with a large surface area (~230 m^2/g) and low pore diameter (~16 nm) was obtained when the powder was processed at pH ~4. The crystallite sizes of the powders processed at pH ~4 and 10, were found to be 35 and 198 nm, respectively. The structural, chemical and thermal studies of the powders were characterized by X-ray diffraction (XRD), Fourier transformed infrared spectrophotometer (FTIR), Carbon analyzer and Thermogravimetry (TGA). High resolution transmission electron microscopic (HRTEM) study of heat treated powders showed a polygonal morphology with particle size of 40 nm when powder was derived at pH ~4. Observations of fluorescence suggested that the $^5D_0 \rightarrow {}^7F_2$ transition within europium was found to be highly dependent on the initial pH.

Keywords: A. Oxides; B. Chemical synthesis

1. Introduction

It is well known that the yttrium oxide (Y_2O_3) has its application in the lighting industry for Eu:Y_2O_3, the red phosphor of the trichromatic fluorescent lamps [1]. Due to a $^5D_0 \rightarrow {}^7F_2$ transition within europium, Eu: Y_2O_3 shows luminescence properties and emits red light with a wavelength of 611 nm [2]. Industrially, Eu doped Y_2O_3 is prepared by heating a mixture of yttrium and europium oxalates at 1300–1500°C [3]. Single crystal of Y_2O_3 and Eu doped Y_2O_3 (1% mole) is grown by a flame fusion process at high temperature (melting point of yttria is approximately 2100°C) using multi-tube burner [4]. Cho et al. [5] have fabricated the Eu doped Y_2O_3 luminescent thin films in situ on a single crystal sapphire substrate using a pulsed laser deposition technique. However, the Eu doped Y_2O_3 target for laser ablation was prepared by mixing the oxides of metal, which were cold pressed, without binder, into a pellet [5]. The pellet was then sintered at a high temperature (i.e. 1400°C) for 24 h in air. Therefore, It has been observed that the traditional ceramic method requires mixing of two metal salts/oxides at high temperatures (>1400°C). However, it inherently lacks a clear approach for controlling homogeneity, purity of phase, narrow size distribution, de-agglomeration, and microstructural uniformity of the powder.

Chemical wet methods (e.g. emulsion, hydrothermal, hydroxide, sol–gel, or growth control method), enable the preparation of the ideal powders (Y_2O_3/doped Y_2O_3) which address the technological barriers posed by traditionally derived powders [6–8]. Nano or ultrafine particles of metal oxide have several intriguing properties, such as, optical non-linearity, specific heat, magnetic, and dielectric non-linearity, different from those of their micron size counterparts [9–11]. In past decades, these ultrafine particles have been studied extensively, and great attention has been given to the research into the fabrication of ceramic powders. Kang et al. [12] have synthesized the spherical particles of

* Corresponding author. Tel.: +1-814-865-0662; fax: +1-814-863-7967.

E-mail address: psharma1234@hotmail.com (P.K. Sharma).

0022-3697/01/$ - see front matter
PII: S0022-3697(01)00124-X

Eu doped Y_2O_3, with hollow morphology, in the nano range from the colloidal solution of yttrium carbonates and europium nitrates salts, in 0.2 M aqueous solution. Furthermore, the spherical particles (in nano range) with solid morphology were observed when Eu doped Y_2O_3 was codoped by Gd through a solution method in the study of Kang et al. [13]. On the other hand, chemical growth controlled method involves the addition of a surface modifier during the precipitation process. The surface modifier reduces the surface free energy of the particulate to an appropriate level by interaction of the modifier with generated particle surface and leads to small particle size. Such modified particles require low temperature of densification as compared to unmodified particles obtained by ceramic or traditional method [11,14]. Several parameters (e.g. solvent, host precursor, dopant concentration, modifier) which affect the fluorescence properties of the Eu doped Y_2O_3 and have already been illustrated [15,16].

The effect of pH, being one of the important factors among which determines the physical and microstructural characteristics of the powder, is usually ignored. The influence of pH on the powder characteristics (e.g. chemical homogeneity, impurity levels, particle size distribution, surface area, pore diameter and microstructure), has been deeply studied for several metal oxides (e.g. Al_2O_3–ZrO_2, Al_2O_3–TiO_2, PbO–ZrO_2–TiO_2, SiO_2) [17–19]. It has been observed that these characteristics further affect the final properties of powder (e.g. electrochemical, optical and electrical) [10,20,21]. There is no systematic study on the effect of initial pH, on physical and fluorescence properties of Eu doped Y_2O_3. Therefore, in this study we are reporting the preparation of the Eu:Y_2O_3 powders with different particle size, in nano meter scale, by varying the pH condition. The purpose of this study is two-fold. First, it is to determine the influence of pH on the physical properties of Eu doped Y_2O_3 (e.g. surface area, pore diameter, pore volume and microstructure). The second purpose is to assess the optical properties (fluorescence) of Eu doped Y_2O_3 for $^5D_0 \rightarrow {}^7F_2$ transition, which is a characteristic of 'red fluorescence' of europium (III) as a function of pH.

2. Experimental

2.1. Synthesis of the powder

A known amount of $Y(NO_3)_3 \cdot 5H_2O$ (0.044 mole) and $Eu(NO_3)_3$ $5H_2O$ (3 mole% with respect to Y) was dissolved in ethanol (i.e. precursor solution). Another solution (modifier solution) was prepared by dissolving 10 wt% of surface modifier (1:1 mixture of tween-80 and ϵ-caprolactam) with respect to Eu_2O_3/Y_2O_3 in 50 ml of aqueous ammonium hydroxide solution (pH $>$ 10). Stirred the solution for an hour at room temperature. The modifier solution was divided into four parts, and the pH of the solution was adjusted for 4, 6, 8 and 10. Lower pH of the solution was maintained by adding aqueous HCl (0.1 mole). The precursor solution containing salts of Eu and Y, was then added to the modifier solution drop by drop through burette at a controlled rate (10–15 drops/min) with vigorous stirring. A known amount of water (2 mole) was added to the resultant solutions. The solution was then stirred continuously for another 2 h. The obtained gel was subjected to centrifuge at the rate of 6000 rpm for 30 min. The aqueous suspension in the centrifugate was removed by refluxing in toluene. Toluene was removed by evaporation. The resulting powder was dried in the oven at 60°C for 24 h and then heat treated in an air atmosphere at 450°C for 2 h.

2.2. Characterization

Multipoint Brunauer–Emmett–Teller (BET) surface area, pore diameter and pore volume were measured for all the samples with a minimum of five points on micrometrics unit (ASAP 2400). Before surface area measurements, the powder was degassed with a pressure of 20 mtorr at 150°C. The thermal analysis was carried out on a Bähr thermoanalyzer (STA 501) in air from room temperature to 800°C. The Infrared spectrum of the powder was recorded on a Fourier-transformation infrared spectrophotometer (FTIR) (Brucker, IFS 25). The crystalline phase of the powder was determined by X-ray diffractometer (XRD) (Siemens, D-500). The microstructure of particle was observed by high resolution transmission electron microscopy (HRTEM) (Philips, CM 200) operated at 200 kV with a line resolution of 1.4 Å. For HRTEM specimen preparation, the copper grid covered with a very thin film of amorphous carbon was used. The copper grid was dipped in a suspension of examined solution. The fluorescence spectra of the powders were measured with a Hitachi fluorescence spectrometer with a 150 W monochromatized Xenon lamp.

3. Results and discussion

The results of thermal analysis of the powders processed at different pH conditions are shown in Figs. 1–4. The dominant thermal process is observed in the temperature range of 110–550°C, in all of the TGA curves. On the other hand, DTA study also indicates the thermal phenomena, e.g. endothermic and exothermic, in the similar temperature range. TGA curves in Figs. 1–4 do not show any weight loss at the temperature $>$600°C. Initial weight loss in the temperature range of 100–160°C is associated with dehydration (refer to TGA curves). This phenomenon is also noticed in the DTA curve (refer to Figs. 1–4) which indicates the presence of two endothermic peaks in the temperature range of 100–160°C. This dehydration can be predicted in two steps, in which physically-adsorbed water eliminates before more strongly held chemisorbed water [22].

It can also be seen in Figs. 1–4 that the endothermic

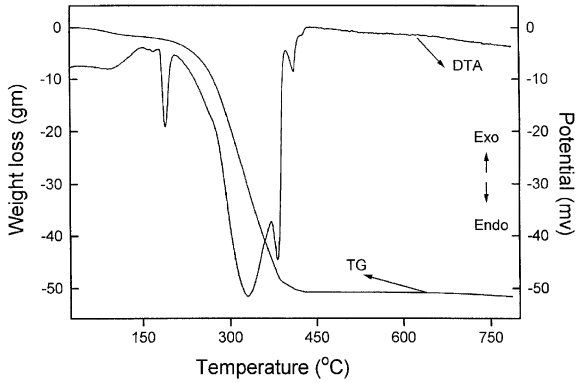

Fig. 1. TGA/DTA curve of the powder prepared at pH 10.

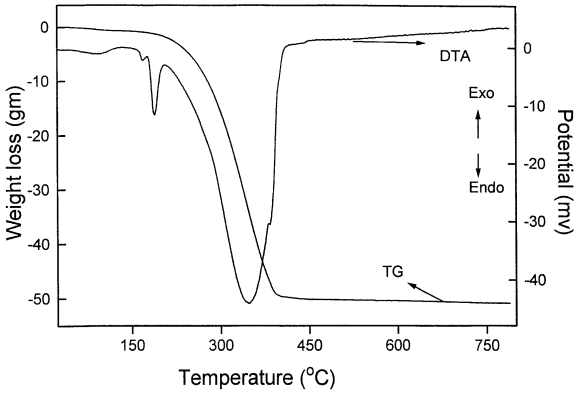

Fig. 2. TGA/DTA curve of the powder prepared at pH 8.

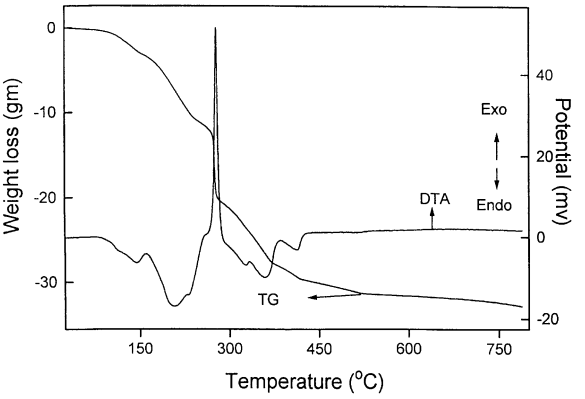

Fig. 3. TGA/DTA curve of the powder prepared at pH 6.

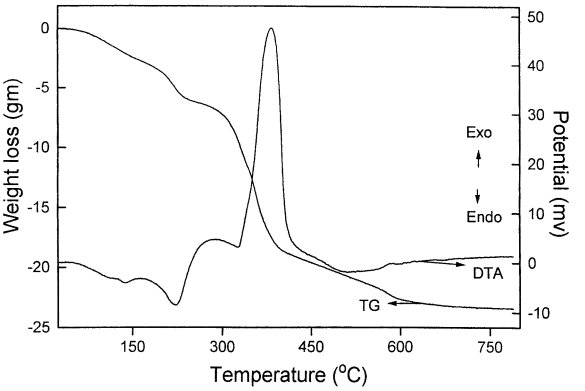

Fig. 4. TGA/DTA curve of the powder prepared at pH 4.

process is found to be dominant in the temperature range of 280 ~ 450°C when the powders derived at pH >7. In contrast, the powders processed at pH <7, are observed to exhibit exothermic reaction profoundly. Endothermic peaks at ~330 and ~430°C appearing in Fig. 1 can be attributed to the partial dehydroxylation and denitration, respectively [20]. Intensity of the peak at ~330°C is found to decreased with decreasing pH, due to the reduction of hydroxyl ions (shown in Fig. 3). This behavior of hydroxyl ions with pH can be illustrated with the help of FTIR spectroscopy and is discussed later.

In Fig. 3 (at pH ~6), a sharp exothermic peak in the temperature range of 290–360°C is visible, which can be assigned to the removal of organic matter. This exothermic process is also accompanied by a corresponding weight loss in the TGA curve (refer to Fig. 3). The broadening of this exothermic peak increases with decreasing pH, as shown in Fig. 4. On the other hand, the exothermic peak in the temperature range of 290–360°C does not appear in the DTA curve of the powder obtained from pH ~10 and 8. However, a corresponding weight loss is observed in the similar temperature range (shown in Figs. 1 and 2). Nevertheless, the existence of carbonaceous matter, which causes the exothermic process, is observed in the FTIR spectra of the powders at pH ~10 and 8 (refer to Fig. 5) and is discussed below. Therefore, absence of such an exothermic peak in the DTA curve (Figs. 1 and 2) can be

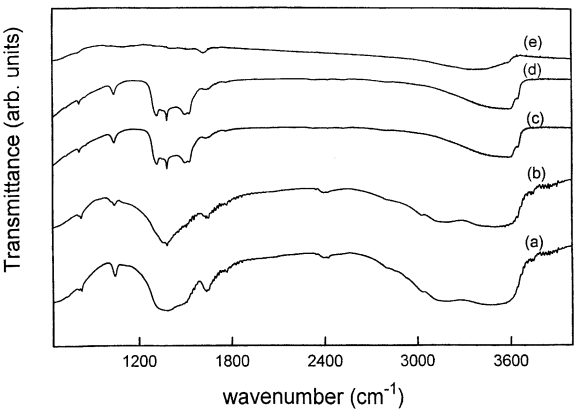

Fig. 5. FTIR spectra of the powders derived (at 350°C) at different pH conditions (a) 10; (b) 8; (c) 6; (d) 4; and (e) 450°C.

Table 1
The effect of pH on chemical and physical properties at 450°C

pH	Carbon content (%)	Surface area (m^2/g)	Pore diameter (nm)	Pore volume (cm^3)
4	0.57	229.06	16.32	0.07
6	0.12	118.24	16.5	0.082
8	0.03	110.89	20.7	0.1
10	0.0	80.37	21.53	0.23

predicted, due to the fact that although an exothermic reaction has occurred, but its presence is masked by one of the endothermic peaks associated with dehydroxylation and denitration. Furthermore, since the temperature region coincides with the endothermic reaction, therefore, exothermic reaction is observed to be dominant only in the powders derived at pH <7.

Fig. 5(a)–(d) shows the FTIR spectra of the powders derived at different pH conditions (4–10). Fig. 5(a) indicates a broad peak at the wavelength region 3300 cm^{-1} and a shoulder at 1685 cm^{-1}, corresponding to OH stretching and bending, respectively. The broadening of the peaks at the region of 3300 and 1685 cm^{-1} is predominant in the powder derived at pH $\backsim$ 10. It has also been observed that the broadening of the peak decreases with decreasing pH value. The peaks at 1380 and 1450 cm^{-1} are assigned to the stretching of C=C and C–C bonds, respectively. Furthermore, the peaks at 1515 and 1420 cm^{-1} are observed, due to the C–O bond stretching and bending, respectively. Additional peaks at 1560,1030 and 820 cm^{-1} are also apparent in the FTIR, which can be assigned to N–O stretching. FTIR spectrum of dried gel (at 350°C) shows that the major constituents of organic matter come from tween-80, ϵ-caprolactam, ethanol, and toluene. In Fig. 5(e), the peak at 3300 cm^{-1} becomes shallow at 450°C, and is an indication of dehydration. The peaks assigned to the stretching of C–H, C–C, and C=C bonds, due to the organic matter, have disappeared at 450°C. It was expected because the organic modifier layer can be maintained up to the temperature ~350°C (refer to Figs. 3 and 4) [16]. But the major peaks in the region of 1100–1500 cm^{-1}, due to N–O and CO_3^{2-}, are still visible. It implies that the final products are assembly metal oxides with some nitrate and carbonate ions on the surface, since they are prepared at the temperature of 450°C. Richard and Akinc [23] have also reported the presence of such bands at a higher temperature for the chemically synthesized yttria powder. Carbon analysis of the powder also indicates the presence of carbon in the powder heat treated at ~450°C (as shown in Table 1). It is obvious because the yttria powder absorbs CO_2 when exposed in air.

It has been observed that the variation in the initial pH has a significant effect on the physical properties of the final product (summarized in the Table 1). Furthermore, the change in physical properties of the powder can only be explained by an understanding of different polymer growth pathways involved in the solution derived at different pH conditions. $M(X_{n-y})(OR)_y$ (where M: Y or Eu) are assumed to be present in the solution, due to the reaction of metal salt (MX_n) and ethanol (ROH: R = C_2H_5). The metal bond with 'OR' group may be readily broken by water, which causes hydrolysis [24]. Therefore, the rate of the reaction is significantly affected by pH.

At low pH, the reaction rate of the hydrolysis is governed by the hydronium ion in solution ($H_2O + H^+ \rightarrow H_3O^+$), and is also observed by Sakka and Kamiya (described below) [25]. In this reaction the amount of water is small due to the rapid formation of H_3O^+. Cagle and Keefer have stated that the hydrolysis/condensation in low pH condition is relatively controlled and selective, thus, generating relatively more linear polymers of metal [26–28]. Hydrolysis can be represented by the following equation

$$\underset{\text{(I)}}{M(X_{n-y})(OR)_y} + H_3O^+ \rightarrow (X_{n-y})(OR)_{y-1} - \underset{\text{(II)}}{M} - (OH) + xH^+ + ROH \quad (1)$$

$$H_2O + H^+ \rightarrow H_3O^+ \quad (2)$$

Condensation can take place by any of the following two equations:

$$(X_{n-y})(OR)_{y-1} - M - (OH) + (OH) - M - (OR)_{y-1}(X_{n-y}) \rightarrow (X_{n-y})(OR)_{y-1} - \underset{\text{(III)}}{M - O} - M - (OR)_{y-1}(X_{n-y}) + H_2O \quad (3)$$

or

$$(X_{n-y})(OR)_{y-1} - M - (OH) + (OR)_{y-1}\, M(X_{n-y})(OH) \rightarrow (X_{n-y})(OR)_{y-1} - \underset{\text{(IV)}}{M - O} - M - (OR)_{y-2}(X_{n-y})(OH) + ROH \quad (4)$$

The linear polymerization can be explained by a simple steric argument: monomers (II) are more readily hydrolyzed than dimers (III or IV), which are in turn more readily hydrolyzed than middle groups in chains. Therefore, the reaction polymerization at low pH is expected to be a linear chain (III or IV) with low cross-links and is also suggested by Pope et al. [29].

At high pH, the reaction is governed by the hydroxyl ions (OH). Although the initial growth leads to linear chains, but

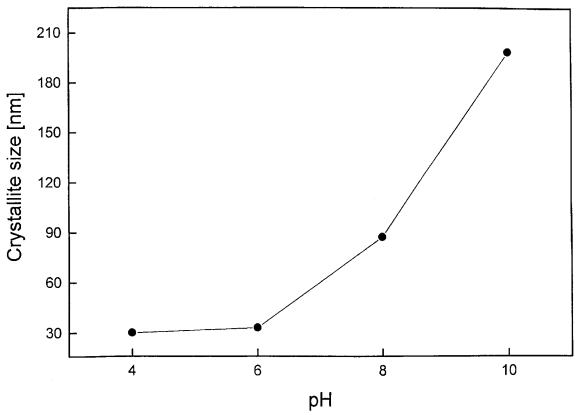

Fig. 6. Effect of pH on the crystallite size of the powder at 450°C.

due to the high concentration of OH

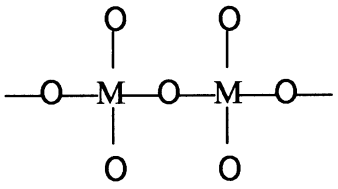

(V) (5)

ions, it results in the cyclization, since the probability of intermolecular reaction is higher than intramolecular reaction [30]. At high pH value, hydrolysis/condensation is uncontrolled and unselective, which leads to highly branched polymers. It also generates larger interconnected particles [17,30,31]. The polymeric chain at high pH is larger than the one at low pH. At high pH, the most probable metal–oxygen polymeric network formed in the chain is the structure V. Nevertheless, the larger interstices at pH >7, result in larger grains, as shown in Fig. 6. Thus, the crystallite size of the powder at pH >7 (198 nm at pH ~10) was smaller than the powder at pH <7 (35 nm at pH ~4). It has been observed that the particle size relation with surface area is inverse, therefore, the surface area of the powder obtained at pH <7 is found to be higher than the powder derived at higher pH [15]. It is in good agreement with the other studies [17].

Furthermore, the effect of pH on the pore size of powders, after heat treatment, is shown in Table 1. Pore size and volume are found to increased with increasing pH (refer to Table 1). In the low pH regime, linear chain growth seems to be preferred, which results in higher reactivity at the chain ends (as 'OR' can easily be replaced by 'OH' group). Linear chains obtained at low pH, have greater flexibility to bend, rotate, and plastically deform after drying, than, the interconnected polymeric chains formed at high pH. As a consequence, the formation of pores after removal of the organic matter is extremely small at low pH. Hence, pore size of the powders obtained from lower pH was 16 nm, in comparison to the one obtained from higher pH (i.e. 21 nm) (refer to Table 1). This correlation of the pore size with pH is consistent with the earlier study [29].

Fig. 7. HRTEM micrograph of the powder prepared at pH ~10 and calcined at 450°C.

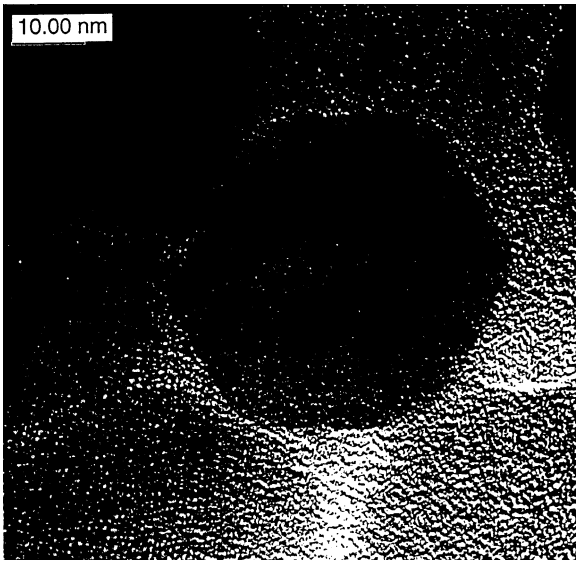

Fig. 8. HRTEM micrograph of the powder prepared at pH ~4 and calcined at 450°C.

It has been noticed that the influence of the pH not only affects the physical properties, but also the morphology of the final product. Figs. 7 and 8 are the HRTEM micrographs of the europium doped yttria synthesized at pH 10 and 4, respectively. At pH ~10, a cube-like morphology of the particles is seen in the Fig. 7. In contrast, the morphology

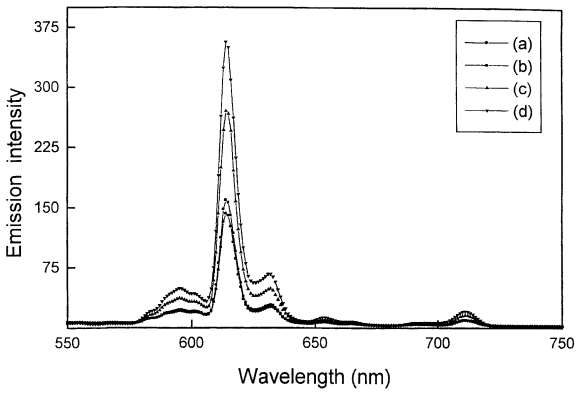

Fig. 9. Complete fluorescence spectra of the powder derived at different pH conditions (a) 10; (b) 8; (c) 6; and (d) 4.

at pH ~4, has totally changed into polygonal shape with size of 40 nm (shown in Fig. 8). This microstructural difference, due to the change in pH, is expected and explained elsewhere [29]. The HRTEM studies indicate that the particle size decreases with decreasing pH value. Our crystallite size measurement also indicates a similar trend.

The rare earth ions, such as Eu^{3+} and Nd^{3+}, show sharp emissions based on electron transitions within the 4f manifold. Further, their emission is found to be highly dependent on the local environment of rare earth ions. Therefore, the fluorescence of Eu^{3+} ions can be used as a probe to investigate the local surrounding in the yttria host that has been prepared by a chemical wet method. Fig. 9 shows the complete fluorescence spectra of Eu doped Y_2O_3 at different pH. It can be seen in the Fig. 10 that the fluorescence emission intensity of $^7F_2$ transition decreases with increasing pH. It reveals the sensitivity of Eu^{3+} fluorescence to the environment, and is attributed to a higher non-radiative path arising, mainly due to the following two reasons. First, Increase in hydroxyl groups in the immediate vicinity of the Eu^{3+} ion [32]. FTIR spectrum in the Fig. 5 clearly shows a constant increase in OH stretching at 3300 cm^{-1} with increasing pH. William et al. [33] have stated that the fluorescence intensity in Nd-silica system is decreased, due to the high concentration of water. Second, pH dependence of fluorescence can also be explained in terms of the crystallite size. Pramod et al. and Bawendi et al. [15,34] have illustrated that the luminescence efficiency is increased with decreasing crystallite size, due to the large surface area of the particle facing the incident light. XRD study of the crystallite reveals that crystallite size decreases from 198 to 35 nm when the pH decreases from 10 to 4. The HRTEM observation of the particle size also indicates a similar behavior with the variation of pH.

4. Conclusion

Based on this study, the following conclusions can be made.

1. Chemical wet process is adopted for the synthesis of Eu(III) doped yttria in the presence of modifier in different pH conditions. The size of the particles can be successfully tailored by using this method. The size and morphology of the particle are greatly influenced by pH conditions. Lower pH is found to be favorable for obtaining a particle at nano size level with uniform morphology.
2. The physical properties such as surface area, pore size and pore volume of the powder can be controlled by the variation of the pH of the solution. It is found that the lower pH (<7) is suitable for obtaining the particles with large surface area, low pore size and volume.
3. Fluorescence study indicates that the emission intensity of $^7F_2$ transition, which is the characteristic of red fluorescence of Eu^{3+}, is sensitive to pH condition. Emission

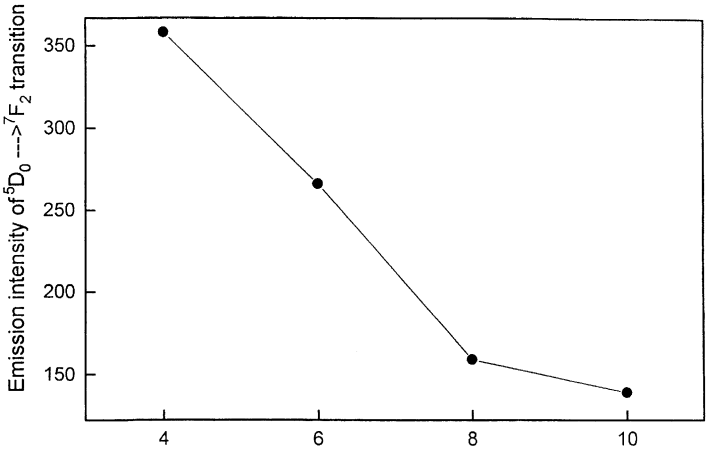

Fig. 10. Effect of pH on the emission intensity of the $^5D_0 \rightarrow {}^7F_2$ transition.

intensity of $^5D_0 \rightarrow {}^7F_2$ transition is increased with decreasing pH value.

References

[1] K.C. Mishra, J.K. Berkowitz, K.H. Johnson, P.C. Schmidt, Phys. Rev. B 45 (1992) 10902.
[2] A. Wickersheim, R.A. Lefever, J. Electrochem. Soc. 111 (1964) 47.
[3] E.F. Apple, Luminescent Materials: in Encyclopedia of Chemical Technology, Of Kirk-Othmer, V-12, 2nd ed, Interscience Publishers, John Wiley & Sons Inc, New York, 1963.
[4] N.C. Chang, J. Appl. Phys. 34 (1963) 3500.
[5] K.G. Cho, D. Kumar, P.H. Holloway, R.K. Singh, Appl. Phys. Lett. 73 (1998) 3058.
[6] L.M. Seaverson, S.Q. Luo, P.L. Chen, J.M. McClelland, J. Am. Cerm. Soc. 69 (1996) 423.
[7] M.D. Rasmussen, M. Akinc, O. Hunter, Cerm. Intern. 11 (1985) 51.
[8] P.K. Sharma, M.H. Jilavi, R. Nass, H. Schmidt, J. Mater. Sci. Lett. 17 (1998) 823.
[9] T. Yazawa, K. Kadono, H. Tanaka, T. Sakaguchi, S. Tsubota, K. Kuraoka, M. Miya, W.D. Xian, J. Non-Cryst. Solids 170 (1994) 105.
[10] C.J. Brinker, G.W. Scherer, Sol–Gel Science: The Physics and Chemistry of Sol–Gel Processing, Academic Press Inc, New York, 1990.
[11] E. Matijevic, Monodispersed colloids: art and science, Langmuir 2 (1986) 12.
[12] Y.C. Kang, S.B. Park, I.W. Lenggoro, K. Okuyoma, J. Mater. Res. 14 (1999) 2611.
[13] Y.C. Kang, H.S. Roh, S.B. Park, Adv. Mater. 12 (2000) 451.
[14] F.F. Lange, J. Am. Cerm. Soc. 72 (1989) 3.
[15] P.K. Sharma, M.H. Jilavi, R. Nass, H. Schmidt, Opt. Mater. 10 (1998) 161.
[16] P.K. Sharma, M.H. Jilavi, R. Nass, H. Schmidt, J. Lum. 82 (1999) 187.
[17] Y-W. Chen, T-M. Yen, C. Li, J. Non-Cryst. Solids 185 (1995) 49.
[18] A.S. Rao, Cerm. Intern. 13 (1987) 233.
[19] R. Coffman, L.R. Barlingay, A. Gupta, S.K. Day, J. Sol–Gel Sci. & Tech. 6 (1996) 83.
[20] E.J.A. Pope, J.D. Mackenzie, J. Non-Cryst. Solids 106 (1986) 236.
[21] P.K. Sharma, V.V. Varadan, V.K. Varadan, Chem. Mater. 9 (2000) 2590.
[22] H. Schmidt, H. Botner, Chemistry and properties of porous organically modified silica, in: Colloid Chemistry of Silica, Advances in Chemistry Series 234, Washington, 1994, p. 419.
[23] K. Richard, M. Akinc, Cerm. Intern. 14 (1988) 101.
[24] B.E. Yoldas, J. Non-Cryst. Solids 83 (1986) 375.
[25] S. Sakka, K. Kamiya, J. Non-Cryst. Solids 48 (1992) 31.
[26] P.C. Cagle, W.G. Klemperer, C.A. Simmons, Molecular Archtectrure and its Role in Silica Sol–Gel Polymerization, in Better Ceramics Through Chemistry III, in: B.J.J Zelinski, C.J., Brinker, D.E. Clark, D.R. Ulrich (Eds.), Mater. Res. Soc. Symp. Proc.,180, Pittsburgh, PA 1990, p. 29.
[27] K.D. Keefer, in: J.M. Zeigler, F.W. Gordon (Eds.), Silicon-based polymer science; A comprehensive resource, Adv. Chem. Ser. 224; Am. Chem. Soc., Washington DC, 1990, p. 228.
[28] L.W. Kelts, N.J. Effinger, S.M. Melpoder, J. Non-Cryst. Solids 83 (1996) 353.
[29] E.J.A. Pope, J.D. Mackenzie, J. Non-Cryst. Solids 87 (1986) 185.
[30] W.G. Klemperer, S.D. Ramamurthi, Molecular growth pathways in Slica Sol–Gel Polymerization, in: C.J. Brinker, D.E. Clark, D.R. Ulrich, Better Ceramics Through Chemistry III, Mater. Res. Soc. Symp. Proc. 121, Pittsburgh, PA, 1988, p. 1.
[31] C. Liu, H. Zhong, S. Komarnani, C.G. Pantano, J. Sol–Gel Sci. & Tech. 1 (1994) 141.
[32] K. Devlin, B. O'Kelly, Z.R. Tang, C. McDonagh, J.F. McGlip, J. Non-Cryst. Solids 135 (1991) 8.
[33] V. Willium, J.-L. Moreshead, R. Nogues, R.H. Krabill, J. Non-Cryst. Solids 121 (1990) 267.
[34] M.G. Bawendi, W.L. Wilson, L. Rothberg, P.J. Carroll, T.M. Jedju, Phys. Rev. Lett. 65 (1990) 1623.